Aerosol vs. Greenhouse Gas Effects on Tropical Cyclone Potential Intensity and the Hydrologic Cycle

Adam H. Sobel,*

Department of Applied Physics and Applied Mathematics and Lamont-Doherty Earth Observatory, Columbia University, New York, New York, USA.

Suzana J. Camargo and Michael Previdi

Lamont-Doherty Earth Observatory, Columbia University, Palisades, New York, USA

**Corresponding author address:* Department of Applied Physics and Applied Mathematics, Columbia University, 500 W. 120th St., Rm. 217, New York, New York, USA.

E-mail: ahs129@columbia.edu

ABSTRACT

Aerosol cooling in the shortwave reduces tropical cyclone (TC) potential intensity (PI) more strongly, by about a factor of two per degree sea surface temperature change, than greenhouse gas warming increases it. This study analyzes single-forcing and historical experiments from the Fifth Coupled Model Intercomparison Project with the goal of a deeper understanding of the physical mechanisms behind this difference. Latent heat flux is used as a proxy for PI, allowing interpretation of PI changes using the surface energy budget. Offline calculations with radiative kernels allow us to estimate what fractions of the surface radiative flux changes can be considered feedbacks due to temperature and water vapor changes. Calculations are carried out for the tropical oceans of each hemisphere (e.g., 0-30N), during the relevant TC seasons. The greater effect of aerosol forcing occurs because shortwave forcing has a greater impact on latent heat flux — and thus also on PI — than does longwave, primarily because of the differences in the direct, temperature-independent component of the surface energy budget response. This result is familiar from prior work on the response of precipitation to radiative forcing, and the essence of the interpretation is similar to that here for PI. We consider only the tropical and seasonal means when studying PI, however, whereas precipitation and the surface energy budget are straightforwardly related only in the global mean. Surface and top-of-atmosphere radiative flux changes with temperature in the two cases (tropical seasonal vs. global annual means) show some quantitatively substantial differences.

1. Introduction

This study addresses the effects of different radiative forcing agents on the potential intensity (PI) of tropical cyclones (TCs). PI is a theoretically-derived quantity (Emanuel 1986, 1995; Bister and Emanuel 1998) that has been shown, with some caveats, to provide a useful upper bound to the actual intensities that TCs can achieve under given environmental conditions (e.g., Bryan and Rotunno 2009a,b). PI also exerts a control on the average intensity of actual TCs even though most do not reach their PI (Emanuel 2000; Wing et al. 2007) (and some may exceed it, e.g., Persing and Montgomery 2003; Hausman et al. 2006; Bryan and Rotunno 2009b; Wang et al. 2014), so that understanding radiative forcing of PI is relevant to understanding how radiative forcing affects actual TC intensities.

Several studies have pointed out that the cooling effect of aerosols should reduce PI, TC activity, or both, either over the Atlantic (Mann and Emanuel 2006; Booth et al. 2012; Dunstone et al. 2013; Ting et al. 2015) or globally (Sobel et al. 2016). Inspired by the results of Ting et al. (2015) for the North Atlantic, Sobel et al. (2016) showed that in simulations from the Fifth Coupled Model Intercomparison Project (CMIP5) of the historical period, considering single-forcing (greenhouse gas-only or aerosol-only) experiments as well as those with all natural and anthropogenic forcings, aerosol-only effects were nearly equal and opposite to greenhouse gas-only effects over most of the historical period, so that the net change in PI in the all-forcing experiments (where both forcings are present, and apparently behave approximately linearly) was small — at least until the most recent couple of decades, when greenhouse gas forcing begins to dominate. This is the case even though the greenhouse gas forcing is substantially larger in absolute terms (i.e., in W m^{-2}) over the entire period, so that the climate warms continuously. Sobel et al. (2016) interpreted this in light of the results of Emanuel and Sobel (2013), who showed in idealized single-column model

(SCM) calculations that imposed changes in the solar constant induce larger changes in PI and precipitation, by approximately a factor of two, than changes in greenhouse gas forcing, when both are measured per degree of sea surface temperature (SST) change. Assuming that the SCM calculations qualitatively represent the physics of the much more comprehensive CMIP5 models well enough for this problem, that solar constant changes are an adequate proxy for aerosol forcing, and that the greenhouse gas forcing exceeds the aerosol forcing in the CMIP5 models by something like a factor of two, the results of Sobel et al. (2016) appear to be broadly consistent with those of Emanuel and Sobel (2013). The physical reasons for the factor of two difference between the impacts of shortwave and longwave forcing on PI, however, remain less than thoroughly explained. In this study, we analyze the same CMIP5 single-forcing experiments in greater detail, with the goal of further clarifying these physical reasons.

Our analysis is closely related to recent studies of the global hydrological cycle. Greenhouse gas warming accelerates the earth's hydrologic cycle and aerosol cooling decelerates it. As in the case of PI, aerosols are about two to three times as effective in changing the hydrologic cycle per degree surface temperature change than are greenhouse gases (e.g., Feichter and Roeckner 2004; Liepert and Previdi 2009); this is relevant, for example, to proposed solar radiation management schemes for ”geoengineering” (e.g., Bala et al. 2008). Some understanding of this difference has been gained by separating changes in the global energy budget into “fast” or “temperature-independent” and “slow” or “temperature-dependent” components (e.g., Andrews et al. 2009, 2010; O'Gorman et al. 2012; Samset et al. 2016). The temperature-independent radiative effect of a given forcing agent at the top of the atmosphere (TOA), or at the surface, is the change in the TOA or surface radiative flux which would occur in the absence of any changes in the global mean surface temperature. In practice, the temperature-independent effect is often estimated as the change which occurs at the very beginning of a simulation in which the radiative forcing agent is switched on abruptly, e.g., using a ”Gregory-type” approach (Gregory et al. 2004), or by running a simulation in which the forcing agent is introduced and SSTs are held fixed. The temperature-dependent effect can be estimated as the change in radiative flux at equilibrium (or some other intermediate state in which there has been a finite temperature change) minus the temperature-independent effect. The temperature-dependent effect depends not only on surface temperature, but also on state variables related to it such as atmospheric temperature and water vapor. These influence TOA and surface radiation through feedbacks that have been extensively defined and documented in the literature, such as the water vapor feedback and lapse rate feedback. Studies with single forcings (e.g., Andrews et al. 2009; Previdi 2010; O'Gorman et al. 2012) show that these temperature-dependent feedbacks are similar for different radiative forcings. The temperature-independent effects of shortwave and longwave forcings, on the other hand, are different, and these differences lead to the differences in the hydrologic cycle response.

The different effects of shortwave and longwave forcings on the global hydrologic cycle can be understood either from the point of view of the tropospheric heat budget or the surface energy budget. In the global mean, over any time scale of interest for climate studies, the tropospheric heat budget requires that the vertically integrated radiative cooling of the atmosphere be balanced by the sum of latent heating due to water condensation and surface sensible heat flux. To the extent that sensible heat flux is small, then, the radiative cooling closely constrains precipitation (Allen and Ingram 2002).

The surface energy budget, on the other hand, requires that the sum of surface latent and sensible heat fluxes balance net surface radiation. To the extent that the surface sensible heat flux is small, surface radiative fluxes constrain precipitation as well since precipitation and surface evaporation must balance in the global mean. While the global mean is essential to make the connection to precipitation, the balance in the surface energy budget itself is local. We show here that PI in the tropics can be understood through similar local surface energy budget arguments, because changes in latent heat flux are good proxies for PI changes. Thus while our analysis bears considerable similarity to those in the hydrologic cycle literature, it differs in our focus on the tropics (that being possible because our arguments do not invoke any global balances), and in particular on individual hemispheres of the tropics during the seasons in which TCs are most active. This changes some of the results quantitatively, and in some respects even qualitatively, from those in the global mean, and we conclude our study with a direct comparison of tropical seasonal and global annual mean results.

2. Models and data

a. Models

We consider here 11 CMIP5 models that have all the simulations and variables available that are necessary for our analysis. The names of the CMIP5 models, number of ensemble members and duration of each simulation are given in Table 1, and the simulations are described in Taylor et al. (2012). The historical simulations are forced with observed time-varying changes in all natural and anthropogenic forcings. The single forcing simulations that we consider are forced with greenhouse gases (GHG) only and aerosols only. The control simulation is the pre-industrial quasi-equilibrium simulation.

The PI is calculated from monthly mean model data, following the definition of Bister and Emanuel (2002), using sea surface temperature, sea level pressure and profiles of temperature and humidity. The net radiative fluxes (shortwave and longwave) at the top of atmosphere and surface were calculated as the difference of the downwelling and upwelling fluxes (i.e. radiative fluxes are positive down), while the surface latent and sensible heat fluxes are positive up.

For all variables and models, the monthly climatology is defined by the 1861-1900 ensemble mean of each simulation category (historical, GHG-only or aerosol-only). The pre-industrial climatology is defined using 100 years (years 101-200) of one ensemble member of that simulation. The anomalies are calculated by subtracting the monthly climatological values for a given simulation from each of the individual ensemble members. The ensemble mean anomalies are defined as the mean of the anomalies over all ensemble members. Seasonal means are defined over the northern hemisphere peak TC season of August - October and the southern TC season of January - March. Area averages in each hemisphere are defined as 0-30N(S). The global means that are shown are also annual means.

b. Radiative Kernels

We compute surface radiative feedbacks due to temperature and water vapor changes in each simulation using the radiative kernel approach (Soden et al. 2008). Feedbacks are thus defined as

$$f_x = \frac{\partial R}{\partial x}\frac{dx}{dT_s} \equiv K_x \frac{dx}{dT_s}, \tag{1}$$

where K_x is the radiative kernel quantifying the change in the surface radiation R due to an incremental change in the feedback variable x (either surface/atmospheric temperature or specific humidity), and dx and dT_s are the changes in the feedback variable and the tropical mean SST over the course of the simulation. We employ the radiative kernels of Previdi (2010) and Previdi and Liepert (2012) that were computed using an offline version of the radiation code from the ECHAM5 general circulation model. The climate response dx is calculated in each simulation as the difference in the monthly climatology between the periods 1861-1900 and 1981-2005, and is regridded to the ECHAM5 grid in order to have the same dimensions as the radiative kernels. The tropical mean SST change is the change between the same two time periods. In the results that follow, we present atmospheric temperature and water vapor feedbacks that have been vertically integrated from the surface to the tropopause, which is taken to be 100 hPa at the equator, increasing linearly to 300 hPa at the poles. These vertically-integrated feedbacks thus represent the net effect of tropospheric column temperature and water vapor changes on the surface radiation.

It is worth noting that since the simulations we analyze include time-varying radiative forcing, and no fixed SST simulations are available for this set of CMIP5 experiments, we are unable to separate the total changes in tropospheric temperature and water vapor occurring in the simulations into fast and slow components. Thus, the tropospheric temperature and water vapor feedbacks that we consider include the effects of any adjustments in these variables that result from the imposed forcing over the course of the simulations.

3. Results

Fig. 1 shows multi-model mean time series of PI and SST for the northern hemisphere tropics from four sets of simulations: historical (all forcings), greenhouse gas-only, aerosol-only, and pre-industrial control. We see that the PI changes in the aerosol-only and greenhouse gas-only runs are approximately equal and opposite, while those in the historical runs — apart from the influence of several volcanoes, which appear as negative excursions lasting a few years — show little trend, at least until the last few decades. In SST, the increases in the greenhouse gas-only simulations clearly exceed in magnitude the decrease in the aerosol-only simulations by about a factor of two, and the historical simulations show an increasing trend over the whole 20th century, though disrupted somewhat by several volcanoes late in the century. These results show, consistently with Sobel et al. (2016) and Emanuel and Sobel (2013), that the aerosol influence on PI per degree SST change exceeds that of greenhouse gases by approximately a factor of two. Individual models, as might be expected, produce noisier time series, and some range in their responses to the forcings (not shown), but do not overall change our impression derived from the multi-model mean.

Fig. 2 shows scatter plots produced from the multi-model mean data, averaged in the same way as in Fig. 1; each point is a different time from the time series. Fig. 2a and 2b scatter SST against PI for August-September-October (ASO) and January-February-March (JFM), and show, as expected, a slope greater in the aerosol-only simulation than the greenhouse gas-only simulation, by about a factor of 2.5.

Figs. 3a-b scatter PI against latent heat flux, and show that the relationships between these two variables are approximately the same for the aerosol-only and greenhouse gas-only experiments, unlike in the SST-PI case shown in Fig. 2. According to theory, PI can be computed as a function of the thermal disequilibrium at the surface:

$$V^2 = \frac{T_s - T_o}{T_o}\frac{C_k}{C_D}(k^* - k), \tag{2}$$

where V is the PI, T_s is the SST, T_o is the outflow temperature, C_k and C_D are bulk exchange coefficients for heat and momentum, and k^* and k are the saturation moist enthalpy of the surface and the actual enthalpy of near-surface air respectively. Equation (2) comes from Bister and Emanuel (1998) and includes the effect of dissipative heating, so that the denominator contains T_o rather than T_s. To understand Fig. 3, however, it does not matter exactly what the factor multiplying the enthalpy difference is. We may simply write

$$V^2 = c(k^* - k) \tag{3}$$

where

$$c = \frac{T_s - T_o}{T_o}\frac{C_k}{C_D},$$

and imagine that changes in SST, outflow temperature, and the exchange coefficients with climate are small, so that c is approximately constant. In that case, PI changes should be controlled by air-sea disequilibrium changes. Further, if surface wind speed changes are also small, then air-sea disequilibrium changes should be proportional to surface turbulent heat flux changes, since those also are proportional to air-sea disequilibrium. If the dominant contribution to the enthalpy difference $k^* - k$ is the latent component, $l_v(q^* - q)$, with q specific humidity and l_v enthalpy of vaporization, with the component related to the temperature difference being small, or the two components can be considered to be proportional to one another, then we can write the latent heat flux E as

$$E \approx d(k^* - k)$$

where the coefficient d contains the surface wind speed as well as an exchange coefficient. Thus if the wind speed can also be assumed constant, we can write

$$V^2 \approx \gamma E, \tag{4}$$

where $\gamma = c/d$. If we consider small perturbations, as in Fig. 3, we can linearize (4) to obtain

$$E' \approx \frac{2\overline{E}}{\overline{V}} V', \tag{5}$$

where V' and E' are the perturbations about basic state values $\overline{V}$ and $\overline{E}$, and we have eliminated γ by noting that $\gamma = \overline{V}^2/\overline{E}$.

The linear relationships and similar slopes in the aerosol-only and greenhouse gas-only experiments suggest that the assumptions used to arrive at (5) are valid to a degree of approximation good enough to be useful for our purpose. We can go one step further, though, and compare the slope itself to the theoretical prediction. The slopes in Fig. 3a are around 2 W m^{-3} s (or W m^{-2} per m s^{-1}), consistent with mean values $\overline{E}/\overline{V} \approx 1$W m^{-3} s. This is somewhat consistent with the mean values of latent heat flux and PI computed from the CMIP5 data, but not precisely so. Domain average values in our northern hemisphere tropical averaging region are 67.4 m s^{-1} for PI and 109.3 W m^{-2} for latent heat flux, and 57.9 m s^{-1} and 116.6 W m^{-2} in the southern hemisphere tropics, giving ratios $\overline{E}/\overline{V}$ around a factor of two larger than our analysis based on Fig. 3a suggests. We suspect this quantitative difference is due to averaging within the large areas over different locations where both PI and surface wind speed vary. We have not attempted to diagnose this further.

Analyses of the SST-PI and latent heat flux-PI slopes from the individual models (Fig. 4) further show that the GHG vs. aerosol differences in the former case are much larger and more consistent than those in the latter. The relationship between latent heat flux and PI is similar across simulations with different forcings, whereas the relationship between SST and PI shows consistent differences between GHG- and aerosol-forced simulations, differences which are our subject here. Considering this and the evidence from Fig. 3, combined with the qualitative agreement with theory, we conclude that it is valid to use the latent heat flux as a proxy for PI for the purpose of explaining the difference in the response of PI to aerosols and greenhouse gases. If we can explain the different relationships between latent heat flux and SST between the aerosol-only and greenhouse gas-only experiments, then, we can take that to be an adequate explanation of the different relationships between PI and SST as well.

The neglect of surface wind speed changes is a caveat on the theoretical interpretation, given that such changes induce larger changes in PI for a given SST change than do surface radiative flux changes (Emanuel and Sobel 2013). But the empirical relationship between latent heat flux and PI on its own justifies using latent heat flux, and thus the surface energy budget overall, to interpret PI responses to radiative forcing, even if the simple theory above does not explain the relationship quantitatively. To the extent that surface wind speeds may change, we can think of PI changes as having a component due to radiative forcings and another component due to wind speed. Our study here aims to explain only the former.

Figs. 5a-h show analogous scatter plots of terms in the surface energy budget — latent heat flux, sensible heat flux, longwave radiative flux, and shortwave radiative flux — vs. SST, for both the northern and southern hemisphere tropics in the respective TC seasons. The conventions are such that the latent and sensible heat fluxes are defined positive up, while the radiative fluxes are defined positive down. Thus in perfect energy balance, the sum of sensible and latent fluxes would equal the sum of the radiative fluxes. The slopes derived from linear regression do not balance in this way; there is an imbalance of ~ 1.1W m^{-2} K^{-1} for the GHG case and 0.9W m^{-2} K^{-1} for the aerosol case in the northern hemisphere for ASO, with the corresponding numbers being 0.6 and 2.2 W m^{-2} K^{-1} for the southern hemisphere in JFM . This may be due to changes in the seasonal cycle - as these are seasonal rather than annual means (e.g., Sobel and Camargo 2011) or changes in ocean heat transport, or imprecision resulting from the regression analysis. In any case, however, the substantial difference in the latent heat flux – SST relationship between the aerosol and greenhouse gas experiments is well explained qualitatively, and to a reasonable extent even quantitatively, by the difference in the radiative terms in those experiments. Summing the slopes from the radiative terms gives ~ 7W m^{-2} K^{-1} for the aerosol vs. 2.5W m^{-2} K^{-1} for the GHG experiments, while the sum of the latent and sensible heat flux slopes is ~ 5W m^{-2} K^{-1} for the aerosol vs. ~ 1.5W m^{-2} K^{-1} for the GHG experiment. A similar degree of agreement is obtained for the historical experiments as well, though the scatter is greater and there is much more cancellation between the two radiative terms. This is roughly consistent with our expectation that the historical experiments can be thought of as a linear sum of the aerosol and GHG experiments. Focusing on the difference between the aerosol and GHG results, we see that the longwave flux into the ocean increases slightly more slowly with SST for the aerosol than the GHG forcing in the northern hemisphere (though not the southern). The difference in the shortwave is much more dramatic, with the shortwave flux into the ocean increasing strongly with SST for the aerosol experiment while it decreases weakly in the GHG experiment, perhaps due to increased shortwave absorption by water vapor.

Fig. 6 shows feedbacks computed from the radiative kernels from the ensemble means of the three sets of experiments, labeled as in the previous figures. Each of the first three columns shows the changes in surface radiative fluxes — longwave, shortwave, and net or the sum of shortwave and longwave (top, middle, and bottom rows respectively) — computed from the changes in a single input variable. The first column shows changes due to surface temperature only, while the second and third show changes due to atmospheric temperature and humidity changes only. The last column shows the sum of all three components, giving the kernels estimates of the total changes in surface radiative fluxes resulting from temperature and water vapor changes.

In Fig. 7 we separate the direct response to radiative forcing agents (greenhouse gases and aerosols) from the feedbacks that result from changes to the climate via surface temperature, atmospheric temperature and atmospheric humidity, using the kernel calculations shown in Fig. 6 to estimate the feedbacks. All quantities shown are values from the late historical period (1981-2005) minus those in the early historical period (1861-1900). Each diamond-shaped symbol indicates changes in SST (horizontal axis) and net latent plus sensible heat flux (vertical axis) for a single model, with colors indicating different experiments as above. The slopes of the lines connecting these multi-model means (solid diamonds) to the origin can be interpreted similarly to the slopes of the scatter plots in Fig. 5. The circles indicate what the changes in latent plus sensible heat flux would be if they were assumed to be equal and opposite to the radiative flux changes inferred from the kernels. That is, we assume in this figure both that the kernels accurately capture the feedbacks due to temperature and humidity changes and that the ocean mixed layer is in equilibrium so that the changes in radiative fluxes are exactly balanced by changes in turbulent fluxes. Under these assumptions, the differences between the circles and the diamonds represent the direct effects of the radiative forcings.

We see from Fig. 7 that not only are the changes in surface turbulent heat fluxes per degree SST change considerably larger for aerosol-only than greenhouse gas-only experiments, but even more so, the components of those changes that we infer to be directly radiatively forced — the difference between the total and the feedback, diamond minus circle — is as well. The feedbacks, on the other hand — apparent here as the slopes of the lines connecting the circles to the origin — are similar between the multi-model means of the greenhouse gas-only and aerosol-only experiments, at least in the northern hemisphere. (In the southern hemisphere, the feedbacks in the aerosol case are mostly consistent with those in the greenhouse gas case, but the multi-model mean is strongly influenced by one extreme outlier.) We interpret the directly forced change as being required by the need for the surface turbulent heat flux to balance the surface radiative flux change that results from the aerosols or greenhouse gases alone; this is referred to as the temperature independent component of the climate response in many studies of the global hydrologic cycle (Andrews et al. 2009, O'Gorman et al. 2012). That this component is larger for shortwave (aerosol) than longwave (greenhouse gas) forcings is consistent with those studies, as is the similarity in the temperature-dependent feedbacks, though these prior studies consider global and annual means while we consider changes over the tropical oceans of single hemispheres in single seasons.

To make a closer connection to the literature on the global hydrologic cycle, Figs. 8 and 9 are analogous to Figs. 5 and 7 except that they show global and annual means.

The results in Figs. 8 and 9 bear some qualitative similarity to those in Figs. 5 and 7, particularly in that the total turbulent flux changes per degree SST are larger for aerosol than greenhouse gas forcing. They are quantitatively different, however. Comparing the scatter plots of latent heat flux vs. SST, the ratio of the slope in the aerosol case to that in the greenhouse gas case is similar in the tropics and globally, on the order of a factor of two in both cases, but both slopes are substantially larger — again by factors between two and three — in the tropical case vs. the global mean. Examination of the radiative fluxes indicates this to be largely a consequence of much larger changes in the tropics than globally, both in the longwave and shortwave. In the case of the shortwave, the differences in the aerosol and greenhouse gas cases between the tropics and globally are not individually as large as are the changes in the longwave, but the difference between the aerosol and greenhouse gas changes is again larger by about a factor of two in the tropics than globally.

Finally, in the interest of understanding the similarities and differences between the global and tropical responses to different radiative forcing agents further, Fig. 10 shows changes in the TOA radiative fluxes, in the same format as figs. 5 and 8, both for the tropics and globally. As above, our sign convention is that all fluxes are positive down.

Fig. 10e shows that in the aerosol experiments, TOA infrared decreases with SST in the global mean, consistent with dominance of the Planck and lapse rate feedbacks over the increasing greenhouse effect associated with increasing water vapor. Net TOA radiation increases slightly with SST, consistent with the SST changes being radiatively forced, due to shortwave TOA flux increases slightly exceeding longwave decreases. This is true as well, though with quantitatively smaller slopes for both longwave and shortwave, in the greenhouse gas experiments (Fig. 10e,f): longwave flux decreases with SST while shortwave increases slightly more. That the net TOA longwave change is negative even in these experiments, where increases in greenhouse gas concentrations are unquestionably the ultimate cause of the warming, may seem counterintuitive, but has been explained previously (Trenberth and Fasullo 2009; Donohoe et al. 2014).

Comparing Figs. 10a and 10c with 10e, in the aerosol case we see much greater scatter in the tropics than globally, and in the northern hemisphere, a much smaller slope, suggesting that the water vapor feedback is more competitive with the Planck and lapse rate feedbacks in that case. In the greenhouse gas experiments, the slopes become clearly positive in the tropics; the water vapor feedback combined with the direct radiative forcing from increasing greenhouse gases dominates. In the shortwave, tropical and global results (Figs. 10b, 10d compared with 10f) show less distinct differences apart from greater scatter in the tropics.

4. Comment on temperature dependence

The CMIP5 results here and in Sobel et al. (2016) appear at first glance consistent with those of Emanuel and Sobel (2013) in that shortwave forcing has a greater influence than longwave forcing on PI per degree SST change. However, close inspection of Fig. 2 in Emanuel and Sobel (2013) shows that, in their radiative-convective equilibrium calculations, the difference emerges only around an SST of around 29°C, higher than the mean values over the regions of interest here. We expect the difference between shortwave and longwave forcings to become greater at sufficiently high SST, since at sufficiently high SST the net surface longwave flux will approach zero as the atmospheric boundary layer becomes very opaque in the longwave while the SST and near-surface atmospheric temperatures are nearly equal. Then further increases in greenhouse gases will have no effect at the surface, and all temperature-dependent longwave feedbacks will approximately vanish there for any forced climate change, while changes in shortwave will still have a substantial temperature-independent effect (though muted somewhat by absorption in the troposphere). This is seen in simulations of precipitation changes in response to changes in tropospheric longwave opacity (representing concentrations of all greenhouse gases including water vapor) over a wide range of climates in an intermediate complexity global model (O'Gorman and Schneider 2008), where precipitation increases with global mean surface temperature saturate at high temperatures.

We interpret the greater sensitivity to aerosols than greenhouse gases in the CMIP5 simulations shown above as being due to qualitatively the same physics as occurs in the higher-temperature regime in Emanuel and Sobel (2013) and (with the caveat again that ours are tropical rather than global results, making quantitative comparison more difficult) O'Gorman and Schneider (2008). Although the difference is manifest at lower SST here than in Emanuel and Sobel (2013), the precise SST at which it should emerge is expected to depend on the details of radiative transfer in both the longwave and shortwave (the latter since shortwave absorption is not negligible) and how both scale with surface temperature. These may differ in different models and experimental designs, all of which are substantially different between the studies described in this section. More detailed study of the surface energy budget's different responses to warming as they depend on these details would be valuable.

5. Conclusions

We have analyzed single-forcing and historical CMIP5 experiments in order to understand the greater influence of aerosols compared to greenhouse gases on the potential intensity (PI) of tropical cyclones (TCs). We analyzed sea surface temperature (SST), PI, and terms in the surface energy budget over the tropical ocean regions and seasons most conducive to TCs. Our primary conclusions are as follows:

1. The variation of latent heat flux with PI is quantitatively similar between aerosol-only and greenhouse gas-only experiments, whereas both PI and latent heat flux vary more strongly with SST, by a factor of two or more, in aerosol-only experiments than in greenhouse gas-only experiments. Thus latent heat flux can be used as a proxy for PI, as we expect from theory if wind speed changes are small. This allows us to use the surface energy budget to understand PI changes.

2. Aerosols have a stronger influence than greenhouse gases because they act primarily in the shortwave part of the electromagnetic spectrum while greenhouse gases act in the longwave.

3. Calculations with offline radiative kernels indicate that the temperature-dependent feedbacks resulting from both temperature and humidity changes are similar between aerosol-only and greenhouse gas-only experiments. This is true in both the longwave and shortwave. Thus the difference between aerosol and greenhouse gas forcings is due to the difference in the direct, temperature-independent effects of the radiative forcing agents themselves.

4. Our results are in most respects qualitatively similar to those from prior studies on the global hydrological cycle. Our analysis differs from those prior ones, however, in that we analyze means over the tropics of a single hemisphere in a single season, as opposed to the global and annual means used in most studies of the hydrologic cycle. Precipitation can be straightforwardly related to radiative quantities only in the global mean, whereas the relationship between latent heat flux and PI, and between latent heat flux and the other terms in the surface energy budget, is local as long as the ocean mixed layer is in an appropriately defined equilibrium on the time scales of interest. Comparison of tropical seasonal results to global annual results for the same CMIP5 experiments, at both the surface and top of atmosphere, shows a number of quantitative differences and even some qualitative ones. As an example, while the net top of atmosphere longwave radiation decreases with SST globally in the GHG experiments (so that the warming is driven by shortwave radiation changes despite the ultimate cause being greenhouse gases, as found by prior studies), it increases with SST in the tropics.

5. Results from historical simulations containing all natural and anthropogenic forcings are complex, with greater scatter in the relationships between the different quantities analyzed here,

and in some respects not obviously predictable a priori from the single-forcing experiments. In general they resemble the greenhouse gas-only experiments more than the aerosol-only experiments, as perhaps might be expected since the greenhouse gas forcing is generally larger than the aerosol forcing over the period simulated. The latent heat flux and PI changes, however, are smaller than in the single-forcing experiments, due to the cancellation between the forcings that motivated this study.

Acknowledgments. AHS and SJC acknowledge partial support from NOAA MAPP grant NA15OAR43100095. We thank Kerry Emanuel and Nadir Jeevangee for helpful discussions, and Prof. Emanuel for comments on the manuscript as well.

References

Allen, M. R., and W. J. Ingram, 2002: Constraints on future changes in climate and the hydrologic cycle. *Nature*, **419**, 224–232.

Andrews, T., P. M. Forster, and J. M. Gregory, 2009: A surface energy perspective on climate change. *J. Climate*, **22**, 2557–2570.

Bala, G., P. B. Duffy, and K. E. Taylor, 2008: Impact of geoengineering schemes on the global hydrological cycle. *Proceedings of the National Academy of Sciences*, **105 (22)**, 7664–7669, doi: 10.1073/pnas.0711648105, URL http://www.pnas.org/content/105/22/7664, http://www.pnas.org/content/105/22/7664.full.pdf.

Bister, M., and K. A. Emanuel, 1998: Dissipative heating and hurricane intensity. *Meteor. Atmos. Phys.*, **50**, 233–240,.

Bister, M., and K. A. Emanuel, 2002: Low frequency variability of tropical cyclone potential intensity 1. Interannual to interdecadal variability. *J. Geophys. Res.*, **107**, doi:10.1029/2001JD000 776,.

Booth, B. B. B., N. J. Dunstone, P. R. Halloran, T. Andrews, and N. Bellouin, 2012: Aerosols implicated as a prime driver of twentieth-century North Atlantic climate variability. *Nature*, doi: :10.1038/nature10946.

Bryan, G. H., and R. Rotunno, 2009a: Evaluation of an analytical model for the maximum intensity of tropical cyclones. *J. Atmos. Sci.*, **66**, 3042–3060.

Bryan, G. H., and R. Rotunno, 2009b: The maximum intensity of tropical cyclones in axisymmetric numerical model simulations. *Mon. Wea. Rev.*, **137**, 1770–1789.

Donohoe, A., K. C. Armour, A. G. Pendergrass, and D. S. Battisti, 2014: Radiative feedbacks on global precipitation. *Proc. Nat. Acad. Sci.*, **111**, 16 700–16 705, doi:10.1007/s00382-014-2308-0.

Dunstone, N. J., D. M. Smith, B. B. B. Booth, L. Hermanson, and R. Eade, 2013: Anthropogenic aerosol forcing of Atlantic tropical storms. *Nature Geosci.*, **6**, 534–539, doi: doi:10.1038/Ngeo1854.

Emanuel, K. A., 1986: An air-sea interaction theory for tropical cyclones. Part I: Steady maintenance. *J. Atmos. Sci.*, **43**, 585–604.

Emanuel, K. A., 1995: The behavior of a simple hurricane model using a convective scheme based on subcloud-layer entropy equilibrium. *J. Atmos. Sci.*, **52**, 3960–3968.

Emanuel, K. A., 2000: A statistical analysis of tropical cyclone intensity. *Mon. Wea. Rev.*, **128**, 1139–1152.

Emanuel, K. A., and A. H. Sobel, 2013: Response of tropical sea surface temperature, precipitation, and tropical cyclone-related variables to changes in global and local forcing. *J. Adv. Model. Earth Sys.*, **5**, 447–458.

Feichter, J., and E. Roeckner, 2004: Nonlinear aspects of the climate response to greenhouse gas and aerosol forcing. *J. Climate*, **17**, 2384–2398.

Gregory, J. M., and Coauthors, 2004: A new method for diagnosing radiative forcing and climate sensitivity. *Geophys. Res. Lett.*, **31**, doi:10.1029/2003GL018747.

Hausman, S. A., K. V. Ooyama, and W. H. Schubert, 2006: Potential vorticity structure of simulated hurricanes. *J. Atmos. Sci.*, **63**, 87–108, doi:10.1175/JAS3601.1.

Liepert, B. G., and M. Previdi, 2009: Do models and observations disagree on the rainfall response to global warming? *J. Climate*, **22**, 3156–3166.

Mann, M. E., and K. A. Emanuel, 2006: Atlantic hurricane trends linked to climate change. *EOS*, **71**, doi:10.1029/2006EO240001.

O'Gorman, P., and T. Schneider, 2008: The hydrological cycle over a wide range of climates simulated with an idealized GCM. *J. Climate*, **21**, 524–535.

O'Gorman, P. A., R. P. Allan, M. P. Byrne, and M. Previdi, 2012: Energetic constraints on precipitation under climate change. *Surv. Geophys.*, **33**, 585–608, doi:10.1007/s10712-011-9159-6.

Persing, J., and M. T. Montgomery, 2003: Hurricane superintensity. *J. Atmos. Sci.*, **60**, 2349–2371.

Previdi, M., 2010: Radiative feedbacks on global precipitation. *Environ. Res. Lett.*, **5**, 025 211.

Previdi, M., and B. G. Liepert, 2012: The vertical distribution of climate forcings and feedbacks from the surface to top of atmosphere. *Climate Dyn.*, **39**, 941–951.

Samset, B. H., and coauthors, 2016: Fast and slow precipitation responses to individual climate forcers: A PDRMIP multimodel study. *Geophys. Res. Lett.*, **43**, doi:10.1002/2016GL068064.

Sobel, A. H., and S. J. Camargo, 2011: Projected future seasonal changes in tropical summer climate. *Journal of Climate*, **24 (2)**, 473–487.

Sobel, A. H., S. J. Camargo, T. M. Hall, C.-Y. Lee, M. K. Tippett, and A. A. Wing, 2016: Human influence on tropical cyclone intensity. *Science*, **353**, 242–246, doi:10.1126/science.aaf6574.

Soden, B. J., I. M. Held, R. Colman, K. M. Shell, J. T. Kiehl, and C. A. Shields, 2008: Quantifying climate feedbacks using radiative kernels. *J. Climate*, **21**, 3504–3520.

Taylor, K. E., R. J. Stouffer, and G. A. Meehl, 2012: An overview of CMIP5 and the experiment design. *Bull. Amer. Meteor. Soc.*, **93**, 485–498.

Ting, M., S. J. Camargo, C. Li, and Y. Kushnir, 2015: Natural and forced North Atlantic hurricane potential intensity change in CMIP5 models. *J. Climate*, **28**, 3926–2942, doi:10.1175/JCLI-D-14-00520.1.

Trenberth, K. E., and J. T. Fasullo, 2009: Global warming due to increasing absorbed solar radiation. *Geophys. Res. Lett.*, **36**, doi:10.1029/2009GL037527.

Wang, S., S. J. Camargo, A. H. Sobel, and L. M. Polvani, 2014: Impact of the tropopause temperature on the intensity of tropical cyclones: An idealized study using a mesoscale model. *Journal of the Atmospheric Sciences*, **71 (11)**, 4333–4348.

Wing, A. A., A. H. Sobel, and S. J. Camargo, 2007: The relationship between the potential and actual intensities of tropical cyclones. *Geophys. Res. Lett.*, **34**, doi:10.1029/2006GL028 581.

LIST OF TABLES

TABLE 1. CMIP5 models acronyms, number of ensembles and each simulations and period of the simulations used in our analysis. Information on the CMIP5 models and simulations can be found in Taylor et al. (2012). The periods of the historical, GHG and aerosols simulations are the same for each model. The climatologies are based on the ensemble mean 1861-1900 average, for the historical, GHG and aerosols simulations and 100 years for the pre-industrial simulations (years 101-200).

Model	Period	Historical	GHG	Aerosols	Years	Pre-Industrial
CanESM2	1850-2005	5	5	5	996	1
CCSM4	1850-2005	6	3	6	501	1
CESM1-CAM5	1850-2005	3	3	3	319	1
CSIRO-Mk3.6.0	1850-2005	10	5	5	500	1
FGOALS-g2	1850-2005	5	1	1	700	1
GFDL-CM3	1860-2005	5	3	3	500	1
GFDL-ESM2M	1861-2005	1	1	1	500	1
GISS-E2-H	1850-2005	10	5	10	240	1
GISS-E2-R	1850-2005	16	5	10	300, 401, 401	3
IPSL-CM5A-LR	1850-2005	5	6	1	1000	1
NorESM1-M	1850-2005	3	1	1	501	1

LIST OF FIGURES

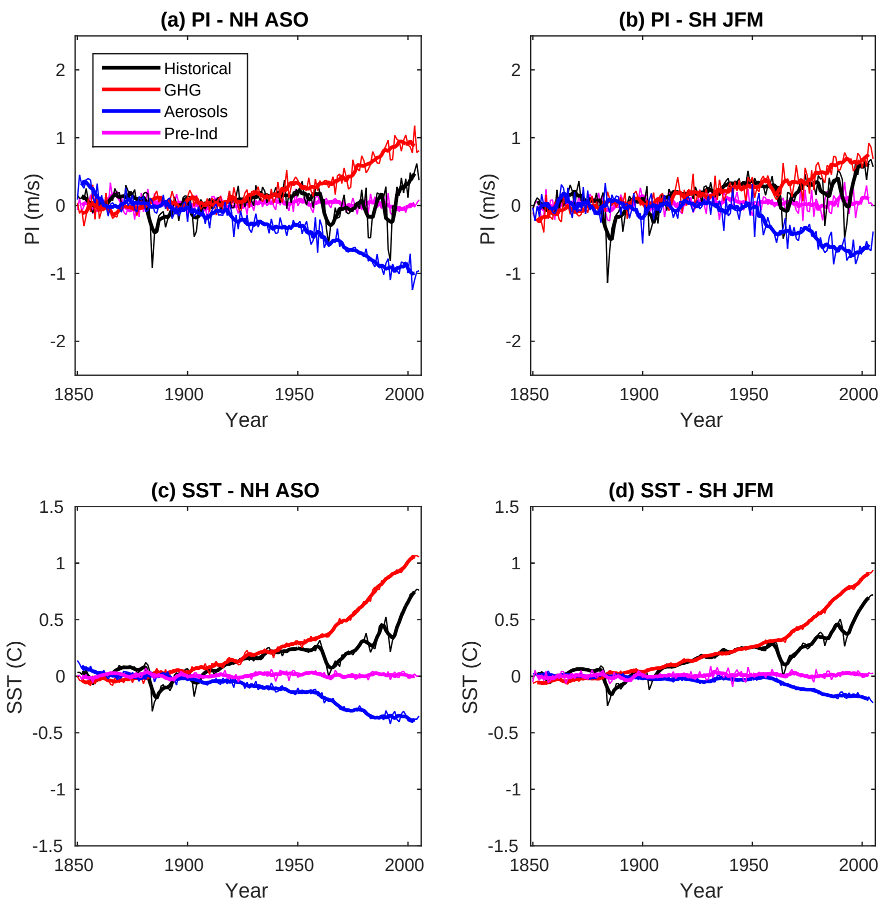

FIG. 1. Time series of multi-model mean potential intensity (a,b) and sea surface temperature (c,d) anomalies in the northern hemisphere tropics (a,c) and southern hemisphere tropics (b,d). Greenhouse gas-only experiments are in red, aerosol-only experiments in blue, and historical experiments in black.

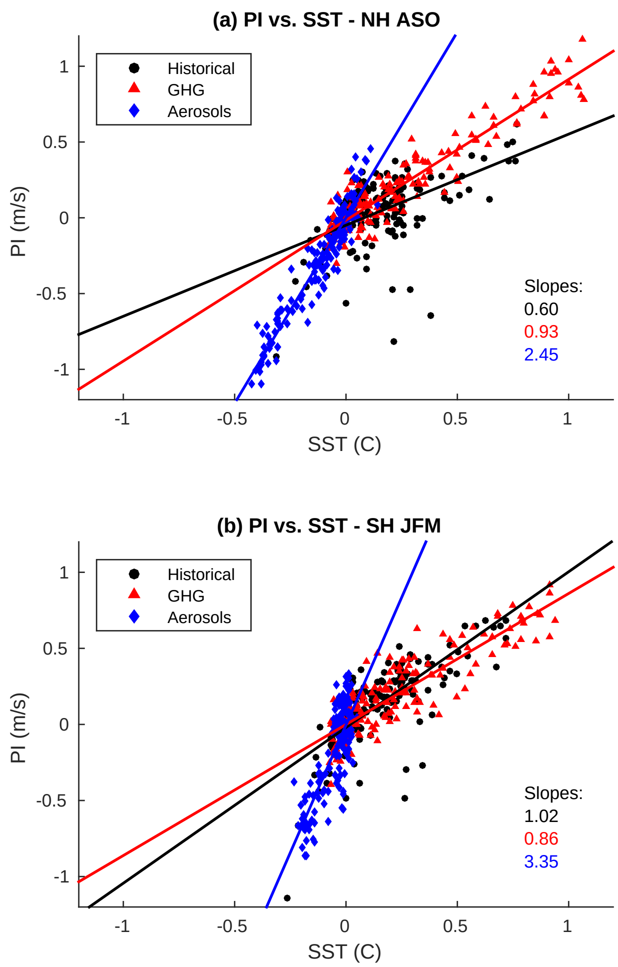

530 FIG. 2. The same data as in Fig. 1, but in the form of scatter plots of SST (horizontal axis) vs. potential intensity (vertical axis). The northern hemisphere is shown in a) and the southern in b). Least-squares regression lines are plotted in the same colors as the associated data, and slopes are given in the lower right area of the plot.

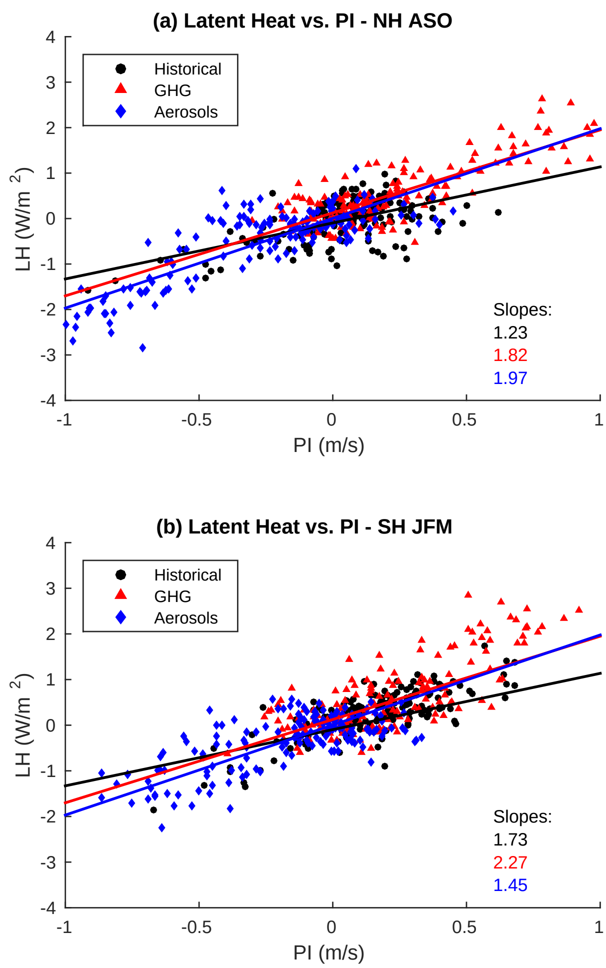

FIG. 3. As in Fig. 2, but for potential intensity (horizontal axis) vs. surface latent heat flux (vertical axis).

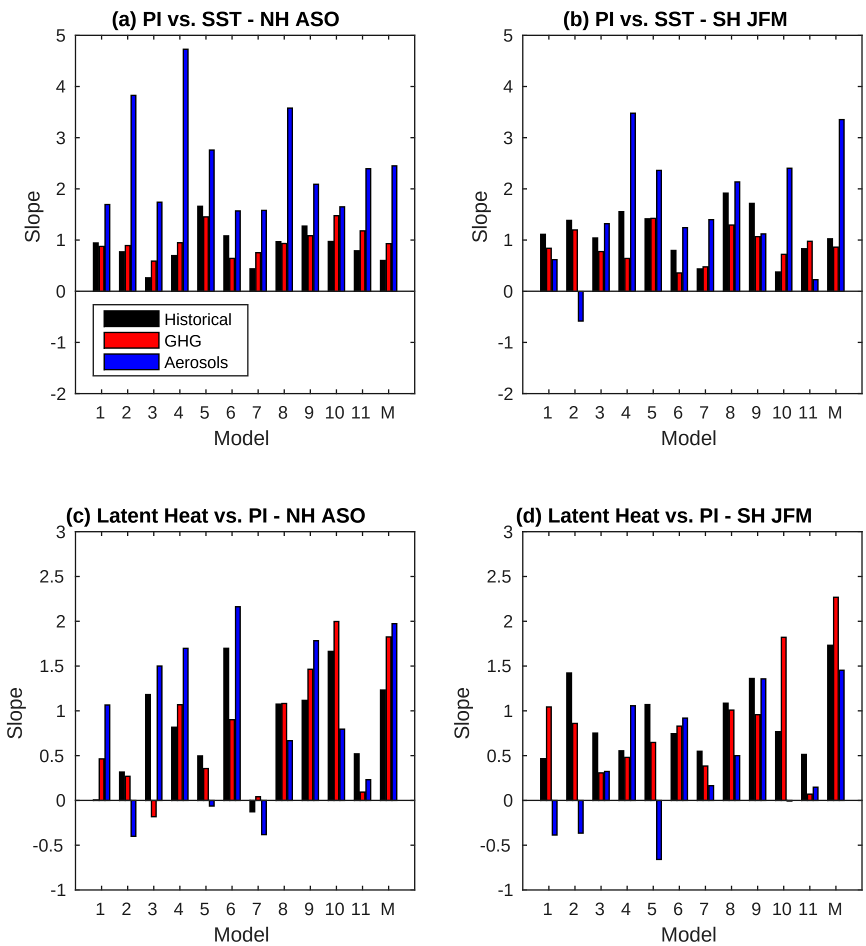

FIG. 4. Bar graph showing regression slopes (m $s^{-1}K^{-1}$) of potential intensity vs. SST (a,b) and potential intensity vs. latent heat flux (c,d), as in Figs. 2 and 3, but made from individual models rather than the multi-model mean; the latter is also shown with the label "M". Color scheme denotes different experiments as in previous figures.

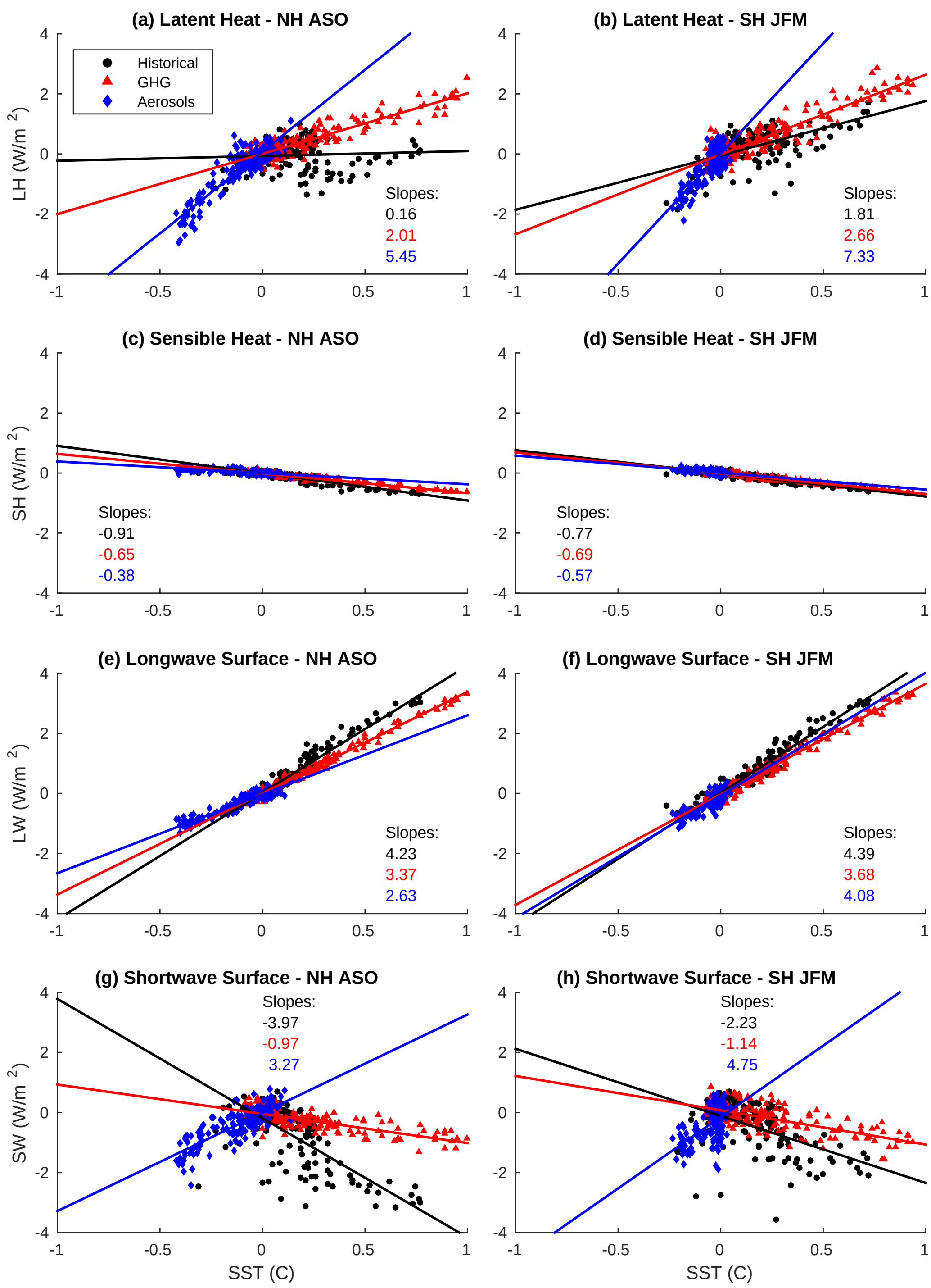

FIG. 5. Scatter plots of multi-model mean surface energy fluxes vs. SST as in Fig. 2. The left column shows results for the northern hemisphere tropics in ASO while the right shows those for the southern hemisphere tropics in JFM. Quantities plotted on the vertical axis are latent heat flux (a,b); sensible heat flux (c,d); net longwave radiative flux (e,f) and net shortwave radiative flux (g,h). Color scheme denotes different experiments as in previous figures.

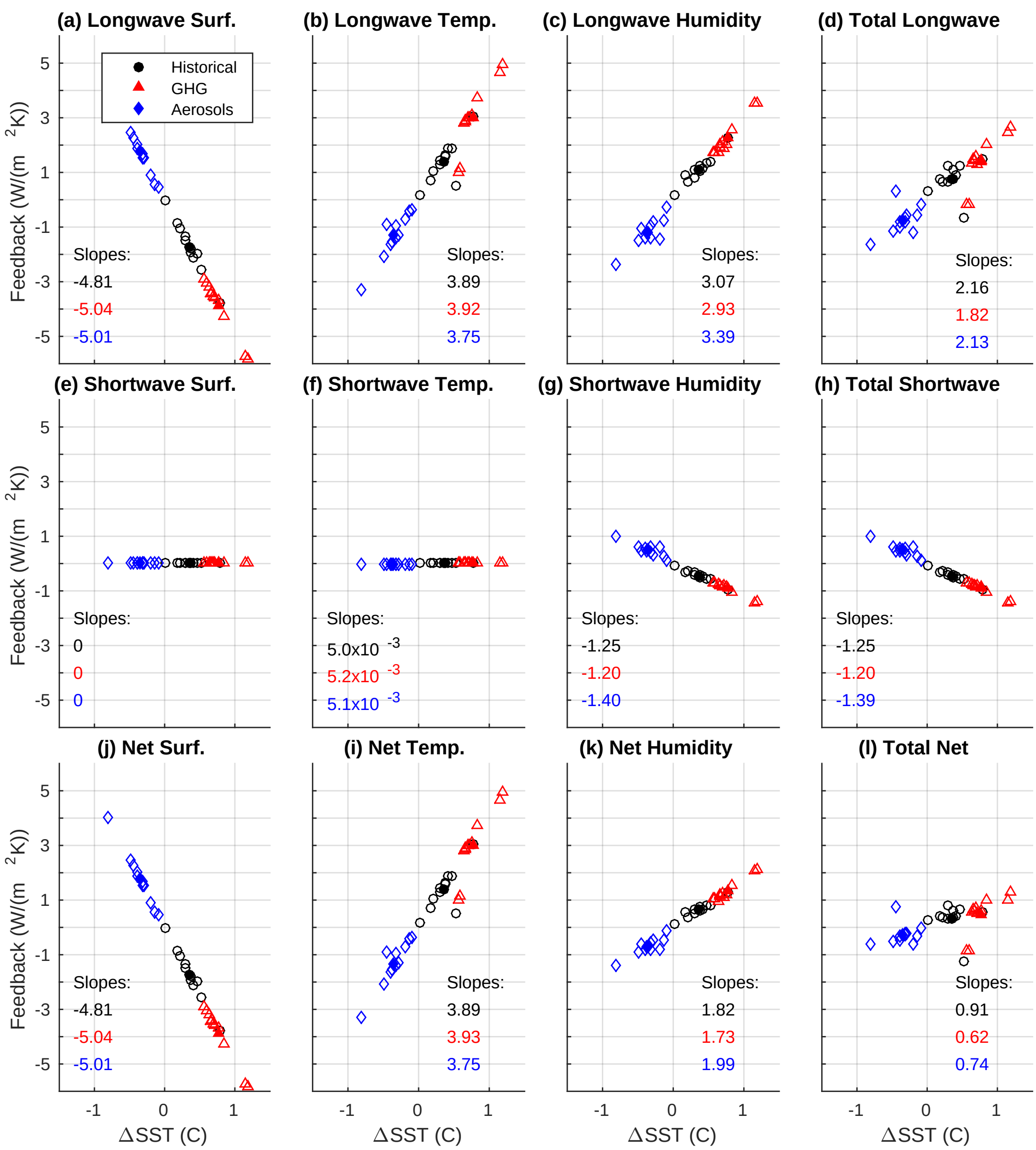

FIG. 6. Feedbacks computed by radiative kernels. Color scheme denotes different experiments as in previous figures. Each open symbol corresponds to the ensemble mean of an individual model, while solid symbols denote multi-model means.

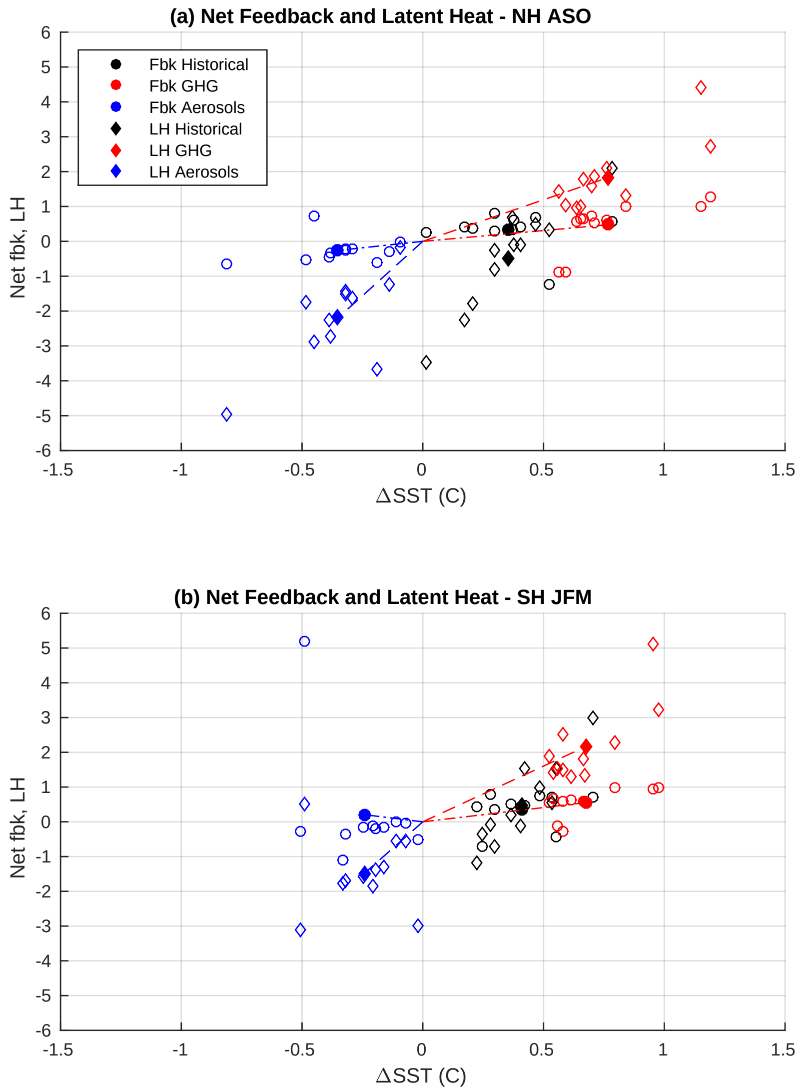

FIG. 7. Changes in net turbulent surface flux (diamonds) and the same quantity estimated from the kernel feedbacks only (circles); see text for details. Individual models are open symbols and filled symbols are multi-model means. Color scheme as in previous figures and shown in legend. Lines are drawn between the origin and the multi-model mean single-forcing results (dashed) and kernel feedbacks (diamonds) as discussed in the text.

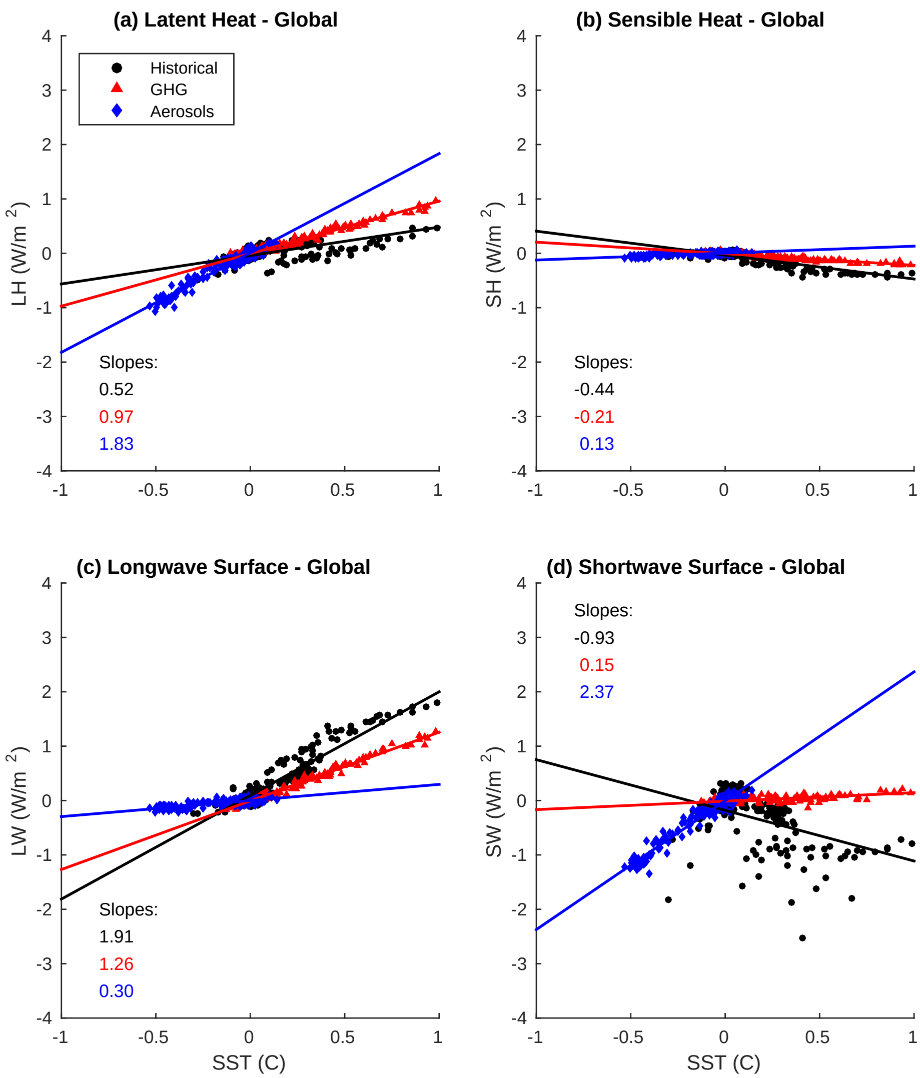

FIG. 8. Scatter plots of longwave and shortwave surface fluxes vs. SST in the global and annual mean.

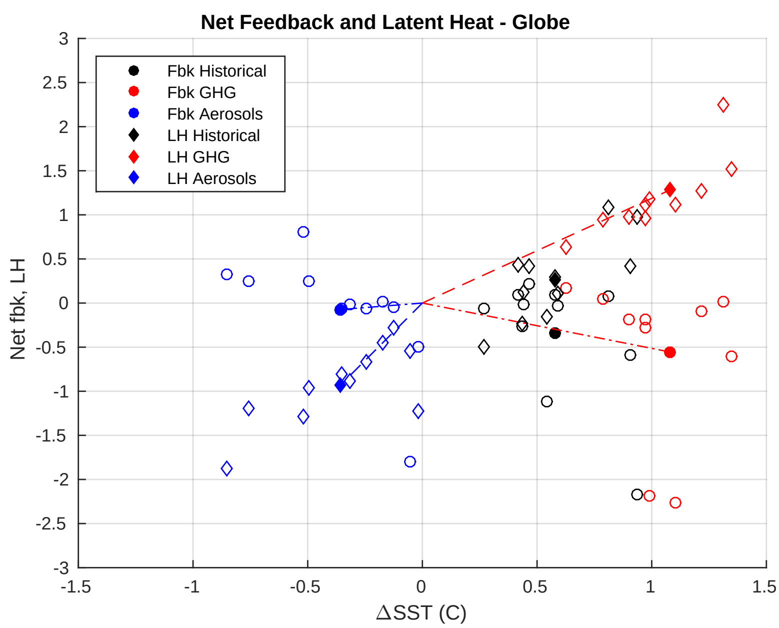

FIG. 9. Analogous to Fig. 7, but for the global and annual mean.

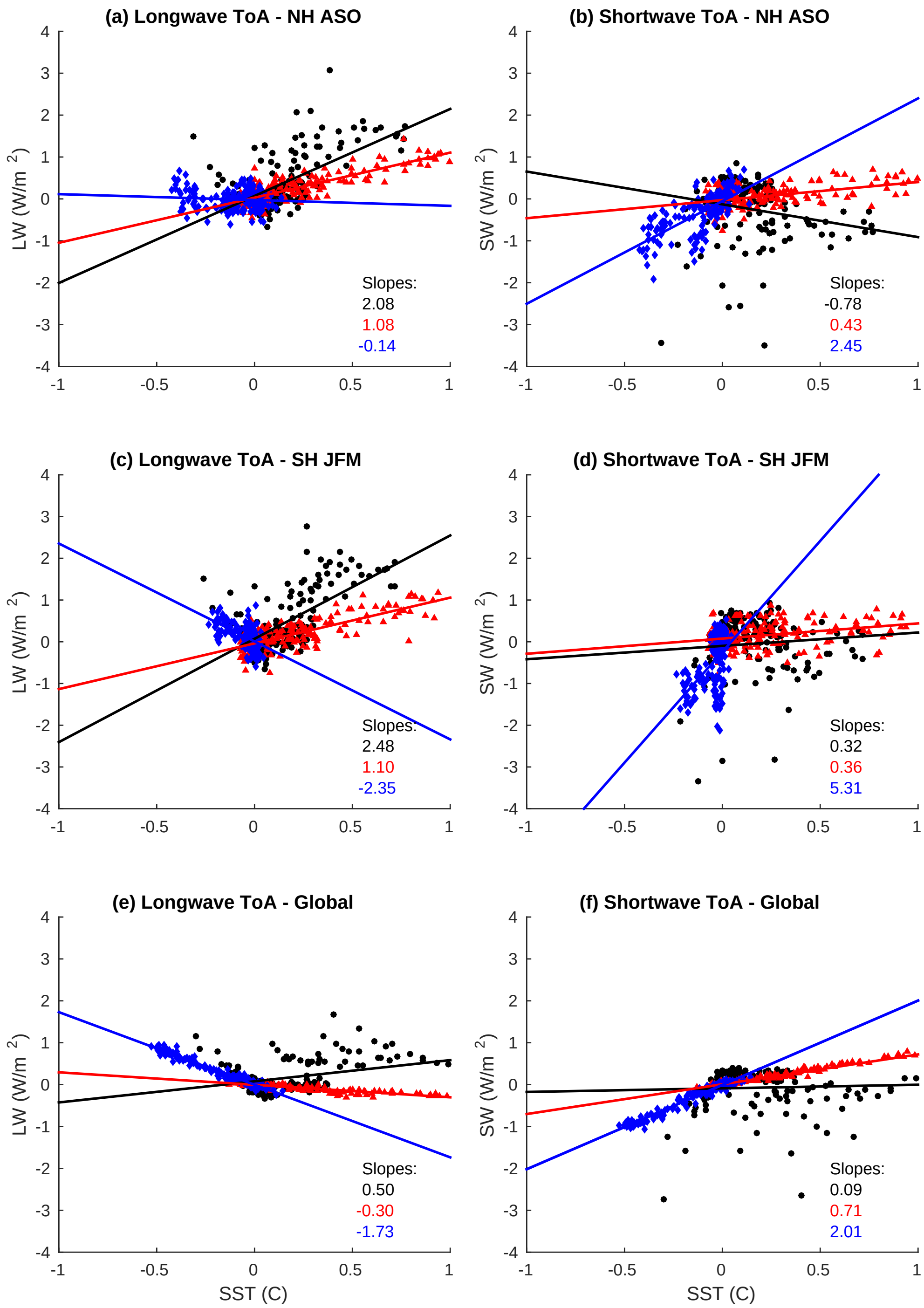

FIG. 10. Scatter plots of top-of-atmosphere radiative fluxes vs. SST for the NH (a,b) and SH (c,d) tropics and the global and annual mean (e,f). Longwave fluxes are on left and shortwave on right.